ACCOUNTS
of chemical research

Critical Interfaces in Organic Solar Cells and Their Influence on the Open-Circuit Voltage

WILLIAM J. POTSCAVAGE, JR., ASHA SHARMA, AND BERNARD KIPPELEN*

Center for Organic Photonics and Electronics (COPE), School of Electrical and Computer Engineering, Georgia Institute of Technology, Atlanta, Georgia 30332

RECEIVED ON MAY 1, 2009

CONSPECTUS

Organic photovoltaics, which convert sunlight into electricity with thin films of organic semiconductors, have been the subject of active research over the past 20 years. The global energy challenge has greatly increased interest in this technology in recent years. Low-temperature processing of organic small molecules from the vapor phase or of polymers from solution can confer organic semiconductors with a critical advantage over inorganic photovoltaic materials since the high-temperature processing requirements of the latter limit the range of substrates on which they can be deposited. Unfortunately, despite significant advances, the power conversion efficiency of organic solar cells remains low, with maximum values in the range of 6%.

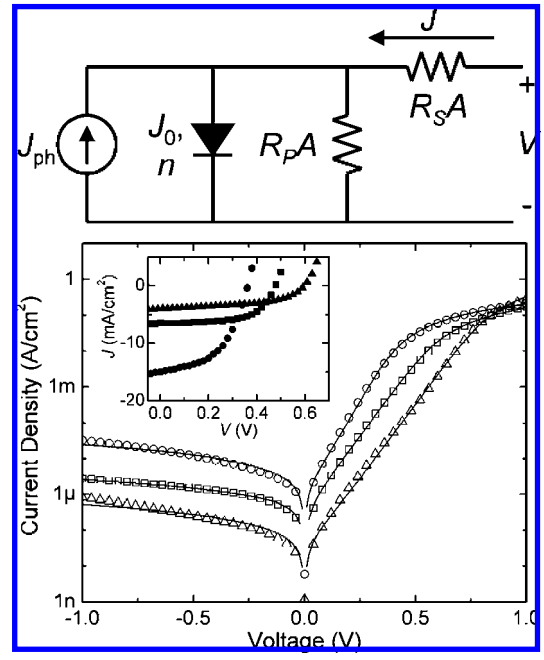

A better understanding of the physical processes that determine the efficiency of organic photovoltaic cells is crucial to enhancing their competitiveness with other thin-film technologies. Maximum values for the photocurrent can be estimated from the light-harvesting capability of the individual molecules or polymers in the device. However, a better understanding of the materials-level processes, particularly those in layer-to-layer interfaces, that determine the open-circuit voltage (V_{OC}) in organic solar cells is critical and remains the subject of active research. The conventional wisdom is to use organic semiconductors with smaller band gaps to harvest a larger portion of the solar spectrum. This method is not always an effective prescription for increasing efficiency: it ignores the fact that the value of V_{OC} is generally decreased in devices employing materials with smaller band gaps, as is the case with inorganic semiconductors.

In this Account, we discuss the influence of the different interfaces formed in organic multilayer photovoltaic devices on the value of V_{OC}; we use pentacene−C_{60} solar cells as a model. In particular, we use top and bottom electrodes with different work function values, finding that V_{OC} is nearly invariant. In contrast, studies on devices incorporating hole-transport layers with different ionization potentials confirm that the value of V_{OC} depends largely on the relative energy levels of the donor and acceptor species that form the essential heterojunction. An analysis of the properties of solar cells using equivalent-circuit methods reveals that V_{OC} is proportional to the logarithm of the ratio of the photocurrent density J_{ph} divided by the reverse saturation current density J_0. Hence, an understanding of the physical origin of J_0 directly yields information on what limits V_{OC}. We assign the physical origin of J_0 to the thermal excitation of carriers from the donor to the acceptor materials that form the organic heterojunction. Finally, we show that the solution to achieving higher power conversion efficiency in organic solar cells will be to control simultaneously the energetics and the electronic coupling between the donor and acceptor materials, in both the ground and excited state.

Published on the Web 08/26/2009 www.pubs.acs.org/acr
10.1021/ar900139v CCC: $71.50

1. Introduction

Organic solar cells have the potential to become ubiquitous power sources that are inexpensive, lightweight, and flexible,[1−3] provided that their power conversion efficiency can be further increased. Compared with inorganic solar cells where the active layers are generally chosen from a small pool of materials, the list of compounds used to make organic solar cells is constantly expanding as previous molecules and polymers are modified to make new compounds with different properties. With so much freedom to modify organic molecules, an understanding of how material properties affect solar cell performance is needed to help guide the design of new compounds. While there is no physical model yet to describe all of the processes in organic solar cells, simple models relating material properties to performance are desirable because they can help in the quest for solar cells with higher efficiencies.

Power conversion efficiency is the most discussed parameter used to evaluate solar cell performance. While many people suggest that an efficiency of at least 10% is necessary for organic solar cells to establish a viable market, the highest efficiencies achieved in organic devices to date are around 5−6%.[4−8] Efficiency is the percentage of input power from the light source that is converted to output power at the operating point where the device produces the maximum power and is written as

$$\eta = \frac{P_{MAX}}{P_{IN}} \times 100\% = \frac{|J_{MAX}|V_{MAX}}{I_L} \times 100\% \qquad (1)$$

where P_{MAX} is the maximum output power, P_{IN} is the input power, J_{MAX} and V_{MAX} are the current density and voltage, respectively, at the point where P_{MAX} is produced, and I_L is the irradiance of the source.

Two other key points of interest are at the boundaries in the current-density−voltage ($J-V$) characteristic where a device begins producing power. Short-circuit current density (J_{SC}) is the current density when the voltage across a device is zero, and open-circuit voltage (V_{OC}) is the voltage when the current density in the device is zero. Because power is the product of current and voltage and either current or voltage is zero at both of these points, there is no power production at either of these points. However, J_{SC} and V_{OC} are useful in that they represent the maximum current density and voltage that can be produced by the illumination of the device.

Efficiency can be rewritten using these two parameters as

$$\eta = \frac{|J_{MAX}|V_{MAX}}{I_L} \times 100\% = FF\frac{|J_{SC}|V_{OC}}{I_L} \times 100\% \qquad (2)$$

with the fill-factor FF defined by

$$FF = \frac{|J_{MAX}|V_{MAX}}{|J_{SC}|V_{OC}} \qquad (3)$$

Figure 1 depicts a typical $J-V$ curve for a device based on a pentacene/C_{60} heterojunction[9−11] in the dark and under illumination with J_{MAX}, V_{MAX}, J_{SC}, and V_{OC} all noted. Bathocuproine (BCP) is used as an interlayer layer between the C_{60} and the Al cathode. The physical processes limiting values for J_{SC} and V_{OC} in organic solar cells must be understood to design new materials for efficient devices because of their relationship to efficiency.

2. Origin of the Short-Circuit Current

The short-circuit current is directly related to the number of photons that are absorbed from the light source to form excitons, the conversion of excitons into electrons and holes, and the efficiency of charge transport to and charge collection at the electrodes. In organic solar cells, absorbed photons lead to bound electron−hole pairs, or excitons. To contribute to the photogenerated current, an exciton must first be dissociated into an electron and a hole. Efficient dissociation can occur at the essential heterojunction formed at the interface between a donor and acceptor material if the exciton binding energy

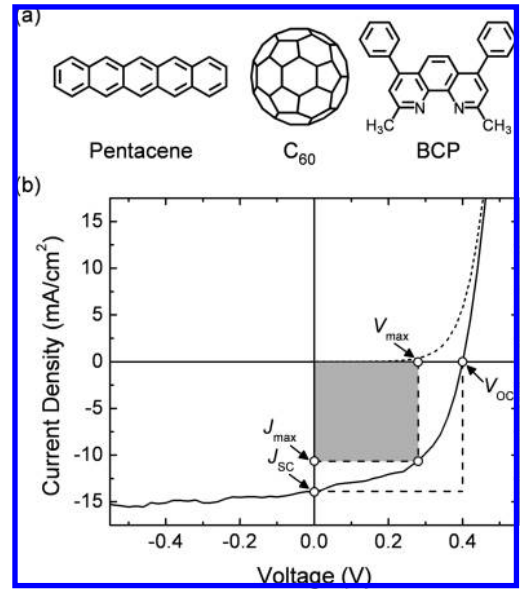

FIGURE 1. (a) Chemical structures of pentacene, C_{60}, and BCP and (b) typical $J-V$ curves for a pentacene/C_{60} device in the dark (dashed line) and in the light (solid line) with key performance parameters noted.

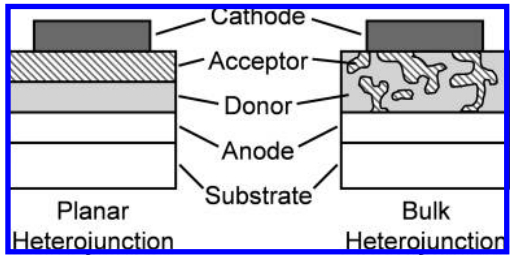

FIGURE 2. Schematics of the basic structures for solar cells based on a planar heterojunction and on a bulk heterojunction.

is less than the energy lost in transferring the electron to the acceptor and the hole to the donor. This interface becomes a charge-injecting contact for electrons and holes on either side of the interface, and carriers travel to their respective electrodes under the gradient of the total electrochemical potential that acts as the driving force and generates the current in the device.

Two main architectures exist for combining the donor and acceptor materials in organic solar cells, as shown in Figure 2: the planar heterojunction[12] and the bulk heterojunction.[13] Planar heterojunctions consist of organic layers sequentially deposited on top of one another and are generally vacuum deposited. With a bulk heterojunction, the donor and acceptor materials are blended together to make an active layer where donor and acceptor interfaces are dispersed throughout the bulk. Bulk heterojunctions benefit from a larger donor−acceptor interface area, potentially resulting in fewer excitons lost to recombination before dissociation. However, the morphology must provide continuous pathways through the donor and acceptor materials for holes and electrons to travel to the electrodes, and getting such a morphology that is thermodynamically stable can be difficult.

In either case, the photocurrent depends on the absorption spectra of the active materials in the device and the spectrum of the light source. While the spectrum of incident sunlight depends on factors such as the location on the earth and cloud coverage, the AM1.5 G solar spectrum shown in Figure 3a is often used as a standard reference spectrum for comparing the efficiency of different solar cells. The dashed line in Figure 3a indicates the amount of current that could be generated if all of the photons up to each wavelength were absorbed and converted into current. The amount of current generated can clearly be increased by broadening the absorption spectra of the active materials in a solar cell with a maximum of ~50 mA/cm^2 available between 300 and 1350 nm.

External quantum efficiency (EQE) defines the percentage of incident photons at a give wavelength that are converted into current. Figure 3b shows the EQE for a device based on a pentacene/C_{60} heterojunction.[14] The J_{SC} that is expected to

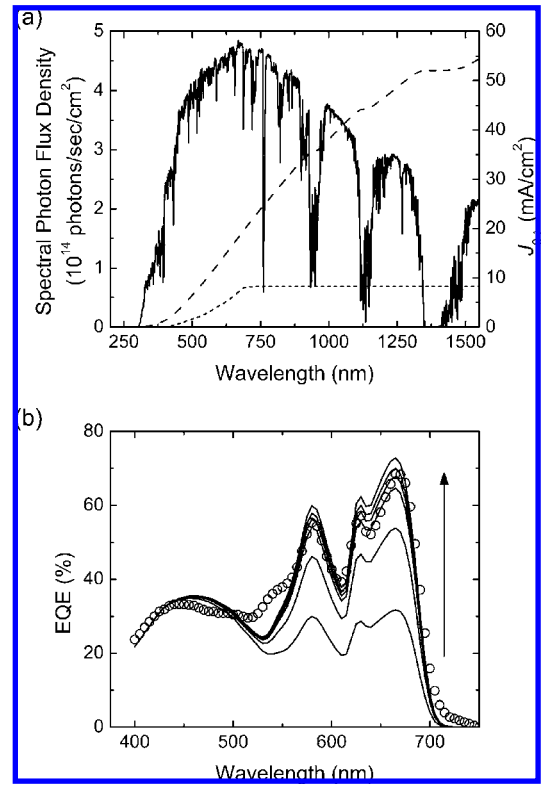

FIGURE 3. (a) Spectral photon flux density of the AM1.5 G solar spectrum (solid line) with the cumulative photon current density from zero up to each wavelength for all of the photons in the spectrum (dashed line) and for the EQE shown in panel b (short-dashed line). (b) Experimental EQE for a pentacene/C_{60} device (symbols) and fits to the model using an exciton diffusion length of 19 nm for C_{60} and varying between 20 and 80 nm for pentacene. The arrow indicates the direction of increasing exciton diffusion length for pentacene.

be generated in a device by a given light source can be calculated by multiplying the EQE with the incident spectrum and integrating. The short-dashed line in Figure 3a shows the cumulative photocurrent density for the pentacene/C_{60} device and the AM1.5 G spectrum. A J_{SC} of 8.2 mA/cm^2 is calculated for this device, and this value does not increase past ~750 nm because of the lack of absorption in the cell after that wavelength.

Because J_{SC} can be calculated from the EQE, models that predict EQE are useful when designing new materials for solar cells. For planar-heterojunction cells, EQE can be modeled by calculating the optical field and exciton distribution in the device using the optical constants, layer thicknesses, and exciton diffusion lengths of the different layers.[14−16] The distribution of excitons is calculated from a one-dimensional diffusion model with the optical field distribution determining the exciton generation rate and the boundary conditions that there are no excitons at the donor−acceptor interface because of efficient separation. Furthermore, a surface recom-

bination velocity can be defined at the boundaries to describe the rate of recombination caused by the interfaces such as those formed with electrodes, but is often assumed in first approximation to be negligible. One additional parameter needed for the diffusion model is the exciton diffusion length, which is the average length an exciton travels before recombination. Finally, the rate of excitons arriving at the interface can be computed from the distribution and related to the current and EQE in the device.[14]

This model can then be used to estimate the exciton diffusion lengths in the materials by fitting the model to experimental EQE with the exciton diffusion lengths as fitting parameters. The solid lines in Figure 3b are EQE spectra calculated using the model with an exciton diffusion length in C_{60} of 19 nm and in pentacene of 20−80 nm.[14] An exciton diffusion length of ~70 nm in pentacene yields EQE spectra that are very close to the experimental data. From the optical data and by assuming values for the exciton diffusion lengths, the EQE and J_{SC} in planar-heterojunction devices can be predicted for new materials.

While this model cannot strictly be applied to bulk-heterojunction devices because of their more complex morphology, the mechanisms leading to current generation in multilayer organic solar cells are fairly well understood. The absorption spectra and exciton diffusion lengths of the organic layers play a key role in determining the J_{SC}. Since efficiency is proportional to J_{SC}, developing materials with low band gaps and broad absorption spectra might seem like the best route for increasing efficiency. However, efficiency is also proportional to V_{OC}, and decreasing the band gap often comes at the expense of decreasing V_{OC}. For this reason, the origin of V_{OC} in organic solar cells must also be studied and better understood.

3. Origin of the Open-Circuit Voltage

The processes governing V_{OC} in organic solar cells are less obvious from a conceptual standpoint than those related to J_{SC} and are still the subject of much debate. By definition, V_{OC} is the voltage across a cell under illumination when there is no current flowing through the device. While there is still a photocurrent being generated by the light, the photocurrent is being offset by other currents in the device, netting zero current flow out of the contacts.

Originally, V_{OC} was thought to be determined by the difference in the work function of the two electrodes used to make a device.[17] More recent studies have shown a correlation between V_{OC} and the difference between the highest occupied molecular orbital (HOMO), or ionization potential, of the donor and the lowest unoccupied molecular orbital (LUMO), or electron affinity, of the acceptor used in both planar-heterojunction[18−20] and bulk-heterojunction[21−25] solar cells. These observations suggest that decreasing the band gap of the organic layers to increase the absorption will also decrease V_{OC} because of a reduced HOMO−LUMO energy difference. More insight into V_{OC} can be gained by studying how material properties affect the $J-V$ characteristics of a device, which ultimately determine the operation of any device.

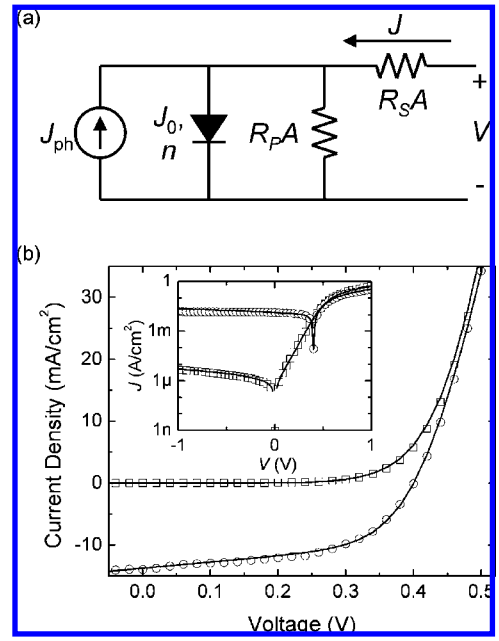

FIGURE 4. (a) Equivalent circuit model for solar cells and (b) fits for a pentacene/C_{60} device in the dark and light using the equivalent circuit model.

3.1. Equivalent Circuit Model. The equivalent circuit model that was originally developed to simulate and understand the $J-V$ characteristics of inorganic solar cells can also be applied to organic solar cells.[26,27] The model uses several basic circuit elements that each account for different processes in a solar cell, and $J-V$ curves can be calculated from the circuit using basic circuit theory. Figure 4a shows a schematic of the equivalent circuit, which consists of a parallel-connected current source, diode, and parallel resistance connected in series with an additional series resistance.

The current source represents the photocurrent J_{ph} generated in the device when under illumination. This term will depend on the spectrum and intensity of the incident light; thus, J_{ph} is zero for a device in the dark. The diode accounts for the rectifying behavior of the donor−acceptor heterojunction and is characterized by the reverse saturation current density J_0 and the ideality factor n. Because diodes follow an exponential curve, the reverse saturation current density is the

current density of an ideal diode when biased with a negative voltage. The ideality factor is related to the slope of the exponential curve, with an ideal diode having an n of unity. Ideality factors greater than unity yield exponential curves that increase more slowly and may be caused by factors such as recombination currents.

The parallel resistance R_PA allows for leakage currents that are not attributed to the diode from sources such as recombination and pinholes. Ideally, R_PA should be high to minimize losses from current circumventing the load. Finally, the series resistance R_SA accounts for the finite resistance of the organic layers and electrodes along with the contact resistance between each of the interfaces. The series resistance prevents the exponential diode from increasing to infinitely large currents and should be small to minimize electrical power losses caused by the resistance limiting the current in the device.

From the equivalent circuit model, the equation for the $J-V$ characteristics of a solar cell can be derived as

$$J = \frac{1}{1 + R_S/R_P}\left[J_0\left\{\exp\left(\frac{V - JR_SA}{nkT/e}\right) - 1\right\} - \left(J_{ph} - \frac{V}{R_PA}\right)\right] \quad (4)$$

where k is the Boltzmann constant, T is the temperature, e is the elementary charge, and A is the area of the device. This equation can be fitted to experimental data using R_S, R_P, J_0, and n as the fitting parameters. Comparison of these parameters for devices with different materials and geometries can then yield information on how the changes affect different aspects of the device.

Figure 4b shows fits to the model in the light and dark for a cell with the geometry indium–tin oxide (ITO)/pentacene (50 nm)/C_{60} (45 nm)/BCP (8 nm)/Al. Looking at the region where the device is producing power from 0 to 0.4 V, the equivalent circuit model closely follows the behavior of the device. Furthermore, the semilogarithmic plots indicate that the model can also fit more than just the power-producing region of the $J-V$ curves with good agreement all the way out to ± 1 V. Details of the fitting procedure can be found elsewhere.[14]

Because of the ability of the model to reproduce the behavior of an actual device, the equivalent circuit can be used to better understand what determines V_{OC}. Open-circuit voltage can be calculated from eq 4 by setting the current to zero and solving for the voltage, yielding

$$\begin{aligned} V_{OC} &= n\frac{kT}{e}\ln\left\{1 + \frac{J_{ph}}{J_0}\left(1 - \frac{V_{OC}}{J_{ph}R_PA}\right)\right\} \quad (5)\\ &\approx n\frac{kT}{e}\ln\left\{1 + \frac{J_{SC}}{J_0}\right\}\\ &\approx n\frac{kT}{e}\ln\left\{\frac{J_{SC}}{J_0}\right\} \end{aligned}$$

with the approximations coming from the assumptions that R_PA is large and R_SA is small. For most good devices, J_{SC} values tend to be within one order of magnitude. Therefore, the parameters with the most impact on the V_{OC} are expected to be J_0 and n.

To investigate what properties of a device affect the J_0 and n and determine V_{OC}, three modifications to interfaces in ITO/pentacene/C_{60}/BCP/Al devices have been carried out in this study. First, the work function of the ITO anode was varied by using different surface modifications. If the work function of the electrodes has the greatest impact on V_{OC}, then changes in both the V_{OC} and circuit parameters can be anticipated. Similarly, the work function of the cathode was varied by using the low work function metal Ca (2.9 eV) in place of Al (4.2 eV). Figure 5 depicts the energy level diagram for a pentacene/C_{60} solar cell and the changes in work function that have been explored by modifying the anode and cathode. Finally, the donor layer was replaced with compounds having different HOMO values, and their effect was analyzed with the equivalent circuit model. All of the device data and efficiencies presented here were measured under illumination of a filtered broadband light source and are not exact values for the AM1.5 G spectrum, but the general trends that are the focus of this Account should hold for AM1.5 G.

3.2. Anode Modification. One way to modify the work function of the anode is through surface modification of the ITO. We have recently reported on the changes in the work function of ITO accomplished by either the incorporation of organic surface modifiers or air plasma treatment.[28−30] The organic modifiers composed of a phosphonic acid moiety, which attaches to the ITO surface, covalently bonded to various dipolar functional groups. Kelvin probe measurements show that the ITO work function can be varied between 4.5 eV for untreated ITO and 5.4 eV for ITO treated with air plasma. Use of pentafluorobenzyl phosphonic acid (F5BPA) on the surface of the ITO resulted in a work function value of 4.9 eV.

Devices were fabricated by vacuum thermal evaporation on top of the modified ITO with the geometry ITO/surface modifier/pentacene (50 nm)/C_{60} (45 nm)/BCP (8 nm)/Al (200 nm). Details about the surface modification and device fabrication

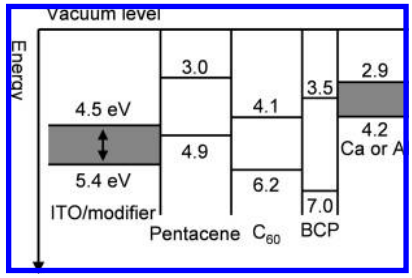

FIGURE 5. Energy level diagram for a pentacene/C_{60} device.

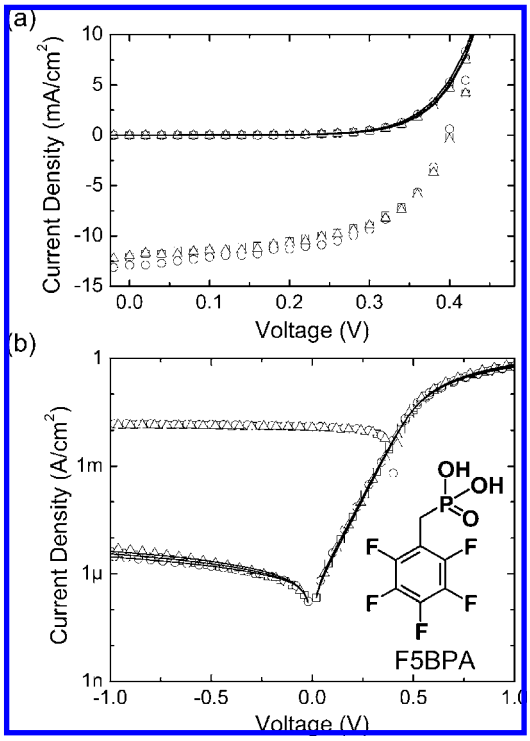

FIGURE 6. (a) Experimental data for pentacene/C_{60} devices on ITO with different surface modifications: unmodified (□), F5BPA (○), and air plasma (△). Solid lines are fits to the circuit model in the dark. (b) The same data on a semilogarithmic plot over a wider range of voltages along with the structure of F5BPA.

can be found in ref 30. Figure 6a shows the $J-V$ characteristics for the devices in the dark and under illumination. Table 1 summarizes the performance parameters for each geometry averaged over three devices. Even with a large change in work function of the ITO, no significant difference in V_{OC}, J_{SC}, or FF is observed.

To verify that changing the work function of the ITO has no effect on the parameters of the equivalent circuit model, experimental data in the dark were fitted to the model. Figure 6b shows the experimental data with the fits using the parameters listed in Table 1. With very little difference between each of the parameters, changing the work function of the ITO with surface modification does not appear to have any significant impact on the device that can be associated with a particular parameter or process. Furthermore, modeling of diodes based on single layers of pentacene sandwiched between modified ITO and Al electrodes suggests that the barrier for injection into the pentacene does not significantly change with the ITO work function, which may be the result of Fermi level pinning.[30]

These results show that the work function of the anode does not necessarily have a strong influence on V_{OC} for organic solar cells. However, the use of different anodes could still significantly alter device performance for other reasons, such as if the morphology of the active layer is modified or if the anode is too resistive.

3.3. Use of Different Cathodes. Next, metals with different work functions were used as the cathode to continue to investigate how the work function difference between the two electrodes affects V_{OC} in organic solar cells. Pentacene/C_{60} devices were made using the same procedures as in ref 30 without any surface modification to the ITO, but either Al or Ca was deposited as the cathode. With a work function of 2.9 eV, Ca has a work function that is 1.3 eV lower than that of Al and should lead to a large increase in V_{OC} if organic solar cells follow the operation of metal−insulator−metal devices.

Figure 7 shows the experimental $J-V$ curves for the devices in the dark and under illumination, and the performance parameters averaged over three samples for each cathode are summarized in Table 2. The devices with Ca as the cathode yield V_{OC} values only 5 mV larger than the Al cathode devices despite the difference of 1.3 eV in work function. Only J_{SC} differs significantly for the Ca devices and is ∼33% smaller than that of the Al devices. The decrease in J_{SC} can be attributed to the lower reflectance of Ca compared with that of Al, which gives less light a second pass through the device and a second chance at absorption.[31] The lower values in V_{OC} and J_{SC} compared with the surface-modified devices are within the range expected for batch-to-batch variations.

TABLE 1. Performance Parameters for Pentacene/C_{60} Solar Cells on ITO with Different Surface Modifications and Fitting Parameters for the Equivalent Circuit Model

surface modifier	V_{OC} (mV)	$\|J_{SC}\|$ (mA/cm^2)	FF	η (%)	J_0 (μA/cm^2)	n	R_SA (Ω cm^2)	R_pA (kΩ cm^2)
unmodified	405 ± 2	13 ± 1	0.55 ± 0.01	3.8 ± 0.1	0.225	1.53	0.648	298
F5BPA	399 ± 2	13 ± 0.2	0.55 ± 0.01	3.7 ± 0.1	0.295	1.56	0.708	375
air plasma	402 ± 1	12 ± 0.4	0.56 ± 0.01	3.6 ± 0.1	0.196	1.52	0.600	247

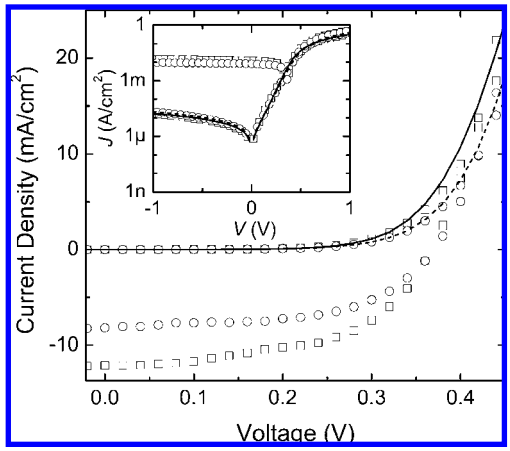

FIGURE 7. Experimental data for pentacene/C_{60} devices with different cathodes: Al (□) and Ca (○). The solid line is a model fit for the Al device and the dashed line for the Ca device. The inset shows the same data on a semilogarithmic scale.

Here again, the equivalent circuit model can be used to more closely evaluate whether the change in cathode had any significant impact on the device that is not obvious by just observing the $J-V$ graphs. Included in Figure 7 are lines calculated from fits to the experimental data in the dark using the parameters in Table 2. Though there is a small difference in J_0 most likely related to batch-to-batch variations, the difference is not large enough to significantly affect V_{OC} because what matters in eq 5 is $\ln(J_{SC}/J_0)$, so much bigger changes in J_0 must be made to impact V_{OC}

3.4. Effect of Donor on Open-Circuit Voltage. Finally, the pentacene layer was replaced with the donors copper phthalocyanine (CuPc) and titanyl phthalocyanine (TiOPc). These donors were chosen because of their difference in HOMO levels, with pentacene having the lowest and TiOPc the highest.[32−34] Figure 8a shows the chemical structures of the phthalocyanines along with the general device architecture used for all of the devices. Details on the device fabrication and testing can be found in ref 35.

Figure 8b shows the $J-V$ curves for the solar cells with the three different donors in the dark and under illumination. Table 3 lists the performance parameters for each device. Open-circuit voltage in these devices increases with the HOMO of the donor. Fits were made by applying the circuit model and are shown in Figure 8b for the parameters in Table 3. The fitting data confirms that J_0 decreases as V_{OC} increases, with a decrease of almost an order of magnitude in J_0 from pentacene to CuPc to TiOPc. While the value of J_0 for this pentacene device is higher than those for previously presented devices, the increase is accompanied by the expected decrease in V_{OC} and may be caused by purity differences in this batch. Clearly, the origin of J_0 must be better understood because of its impact on V_{OC}.

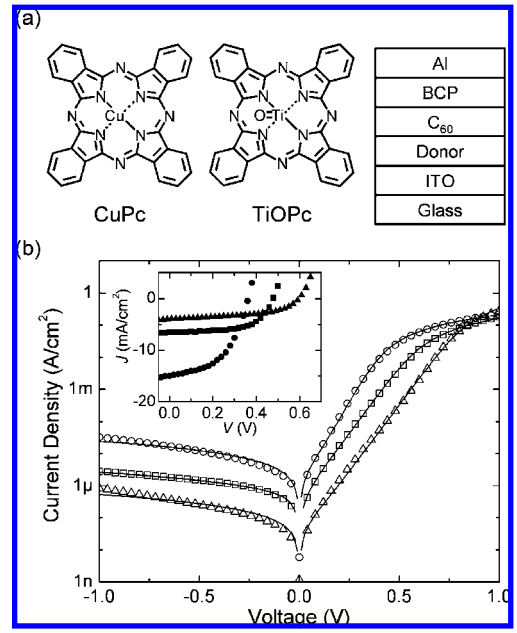

FIGURE 8. (a) Chemical structures of CuPc and TiOPc, and the test structure used for the donor/C_{60} cells. (b) Dark $J-V$ characteristics for donor/C_{60} cells where the donor is either pentacene (○), CuPc (□), or TiOPc (△). The straight lines are fits using the parameters in Table 3. Inset shows $J-V$ curves under illumination for the same devices.

Analysis of J_0 in the dark for the pentacene device revealed that J_0 as a function of temperature, shown in Figure 9, can be fitted with the thermally activated injection expression

$$J_0 = J_{00}\exp\left(\frac{-\phi_B}{kT}\right) = J_{00}\exp\left(\frac{-\Delta E_{HL}}{n'kT}\right) \qquad (6)$$

with an activation energy $\phi_B = 0.55$ eV and a prefactor $J_{00} = 3090$ A/cm^2 over the measured temperature range from 275 to 336 K. The activation energy ϕ_B can be rewritten as $\Delta E_{HL}/n'$, where ΔE_{HL} is the difference between the HOMO of the donor and the LUMO of the acceptor before junction formation and n' is a factor that accounts for effects such as the formation of charge-transfer states[36] and vacuum level misalignments at the heterojunction caused by energy level

TABLE 2. Performance Parameters for Pentacene/C_{60} Solar Cells with Different Cathodes and Fitting Parameters for the Equivalent Circuit Model

cathode	V_{OC} (mV)	$\lvert J_{SC}\rvert$ (mA/cm^2)	FF	η (%)	J_0 (μA/cm^2)	n	R_SA (Ω cm^2)	R_PA (kΩ cm^2)
Ca	371 ± 2	8.1 ± 0.1	0.56 ± 0.01	2.2 ± 0.1	0.615	1.62	1.09	48.4
Al	367 ± 2	12.1 ± 0.4	0.54 ± 0.01	3.1 ± 0.1	0.414	1.46	1.53	60.1

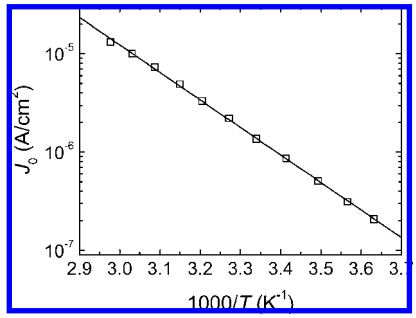

FIGURE 9. J_0 at different temperatures for a pentacene/C_{60} device (□) and fit using eq 6 with $J_{00} = 3090$ A/cm^2 and $\phi_B = 0.55$ eV (solid line).

bending and interface dipoles that reduce the activation energy from ΔE_{HL}.

A final equation for V_{OC} can be obtained using eqs 5 and 6 as

$$eV_{OC} = n\phi_B - nkT \ln\left\{\frac{J_{00}}{J_{SC}}\right\} = \frac{n}{n'}\Delta E_{HL} - nkT \ln\left\{\frac{J_{00}}{J_{SC}}\right\} \quad (7)$$

Values of J_0 and V_{OC} calculated for each of the devices with different ϕ_B are listed in Table 4 and show good agreement with the experimental values. We note that ϕ_B is lower than ΔE_{HL}. This was expected because of various physical processes that can occur at the interface when the donor and acceptor materials are brought into contact. Measured values of the gap at CuPc/C_{60} interfaces of ~0.7 eV agree with the value of 0.6 eV calculated here.[20,37,38]

The first term in eq 7 shows the importance of ΔE_{HL} in influencing V_{OC}, and the second term suggests that V_{OC} will decrease as J_{00} increases. To understand the correlation between molecular structure and the open-circuit voltage in organic solar cells, we turn now to a brief discussion of the physical origin of the reverse saturation current. We had previously assigned its origin to the thermal excitation of carriers at the donor/acceptor heterojunction through a reaction of the type D + A→ $D^+ + A^-$ in which an electron gets transferred from the HOMO of a donor molecule to the LUMO of an acceptor molecule.[35] The rate for such a reaction can be described at the molecular level by a semiclassical Marcus theory expression,

$$k_t = \frac{2\pi}{\hbar}|V_{if}|^2\sqrt{\frac{1}{4\pi\lambda kT}}\exp\left(-\frac{(\Delta G_0 + \lambda)^2}{4\lambda kT}\right) \quad (8)$$

where λ is the reorganization energy induced by the electron transfer, ΔG_0 is the variation of the Gibbs free energy during the reaction, and V_{if} is the electronic coupling matrix element.[39] The steady-state reverse saturation current density can also be written as

$$J_0 = ek_tN_{CT} \quad (9)$$

where e is the elementary charge and N_{CT} is the surface density of interacting donor and acceptor pairs that can be thermally excited with a rate k_t given by eq 8. By combining eqs 6, 8, and 9, the prefactor J_{00} can also be expressed as

$$J_{00} = eN_{CT}\frac{2\pi}{\hbar}|V_{if}|^2\sqrt{\frac{1}{4\pi\lambda kT}} \quad (10)$$

and the thermal activation barrier ϕ_B in eq 6 can be correlated with $(\Delta G_0 + \lambda)^2/(4\lambda)$ in the argument of the exponential term in the Marcus expression in eq 8. This analysis shows that the reverse saturation current density is strongly influenced by the molecular energy levels of the donor and acceptor molecules that form the organic heterojunction. However, eq 10 illustrates that the electronic coupling and reorganization energy are equally important in influencing the reverse saturation current. Hence, as donor and acceptor materials are designed for future high-efficiency organic solar cells, great consideration must be given to their molecular shape, geometry, charge densities, relaxation due to vibrational modes, and packing. The energetics and electronic coupling between donor/acceptor molecules and polymers will simultaneously impact the short-circuit current and the open-circuit voltage. To maximize exciton dissociation, large energy level offsets and a strong electronic coupling are desirable for charge transfer reactions of the type $D^* + A \rightarrow D^+ + A^-$ or $D + A^* \rightarrow D^+ + A^-$ that involve molecules or polymers in the excited state. To achieve large open-circuit voltages, large values for ΔE_{HL} and a weak electronic coupling between the donor and acceptor materials are required for charge transfer reactions of the type $D + A \rightarrow D^+ + A^-$.

TABLE 3. Performance Parameters for Donor/C_{60} Solar Cells with Different Donors and Fitting Parameters for the Equivalent Circuit Model

donor	V_{OC} (mV)	$\lvert J_{SC}\rvert$ (mA/cm^2)	FF	η (%)	J_0 (μA/cm^2)	n	R_SA (Ω cm^2)	R_PA (kΩ cm^2)
pentacene	0.35	11.0	0.53	2.1	1.37	1.68	0.480	110
CuPc	0.47	6.45	0.62	1.9	0.33	2.00	1.98	43.9
TiOPc	0.60	3.99	0.51	1.2	0.023	2.02	0.413	1970

TABLE 4. Values Calculated for Each Donor/C_{60} Cell Using Eq 7 with J_{00} = 3090 A/cm^2, n from Table 3, and T = 300 K for the calculation of J_{0Th} in the dark and 323 K for V_{OCTh} under illumination

donor	ϕ_B (eV)	J_{0Th} (μA/cm^2)	V_{OCTh} (V)
pentacene	0.55	1.55	0.34
CuPc	0.60	0.26	0.47
TiOPc	0.67	0.02	0.59

4. Conclusions

Efficiency of organic solar cells is dependent on both the short-circuit current and the open-circuit voltage of a device. While designing molecules with small band-gaps may be beneficial to absorbing more of the solar spectrum and increasing the short-circuit current, reduced band-gaps may also reduce the open-circuit voltage. We have shown through the use of an equivalent circuit model that the open-circuit voltage is related to the reverse saturation current. In the future, more must be done to understand how material properties affect the reverse saturation current and to create combinations of donor and acceptor molecules that can reduce the reverse saturation current.

This material is based upon work supported in part by Solvay S.A., the STC Program of the National Science Foundation under Agreement Number DMR-0120967, the Office of Naval Research, and the Georgia Research Alliance. The authors thank the Marder group for synthesizing the surface modifier used to modify the work function of ITO and Professor N. R. Armstrong and M. Brumbach for providing the TiOPc device data.

BIOGRAPHICAL INFORMATION

William J. Potscavage, Jr. was born in Houston, TX, in 1982. He earned his B.S. (2003) and M.S. (2005) from the Georgia Institute of Technology and is currently pursuing his Ph.D. there. His interests include developing solar cells based on new polymers and small molecules and investigating the physics of device operation.

Asha Sharma received her Ph.D. from IIT, Kanpur, India, in 2006. Following that, she was a postdoctoral fellow at the Georgia Institute of Technology, Atlanta, at the Center for Organic Photonics and Electronics in the School of ECE until 2008. She is currently a postdoctoral researcher at the University of Utah, Salt Lake City, in the department of Electrical and Computer Engineering where she is working on wireless integrated neural interfaces for biomedical devices.

B. Kippelen received his Ph.D. in solid-state physics in 1990 from the University Louis Pasteur, Strasbourg, France. He was Chargé de Recherches at the CNRS. In 1994, he joined the Optical Sciences Center at The University of Arizona where he became an Assistant Professor in 1998 and an Associate Professor in 2001. Since 2003, he has been Professor of Electrical and Computer Engineering at the Georgia Institute of Technology, Atlanta, GA. He is a Fellow of the Optical Society of America, a Fellow of SPIE, and a Senior Member of IEEE.

FOOTNOTES

*To whom correspondence should be addressed. E-mail address: kippelen@ece.gatech.edu.

REFERENCES

1 Kippelen, B.; Brédas, J.-L. Organic photovoltaics. *Energy Environ. Sci.* **2009**, *2*, 251–261.
2 Dennler, G.; Lungenschmied, C.; Neugebauer, H.; Sariciftci, N. S.; Labouret, A. Flexible, conjugated polymer-fullerene-based bulk-heterojunction solar cells: Basics, encapsulation, and integration. *J. Mater. Res.* **2005**, *20*, 3224–3233.
3 Krebs, F. C.; Spanggard, H.; Kjær, T.; Biancardo, M.; Alstrup, J. Large area plastic solar cell modules. *Mater. Sci. Eng., B* **2007**, *138*, 106–111.
4 Xue, J.; Uchida, S.; Rand, B. P.; Forrest, S. R. Asymmetric tandem organic photovoltaic cells with hybrid planar-mixed molecular heterojunctions. *Appl. Phys. Lett.* **2004**, *85*, 5757–5759.
5 Ma, W.; Yang, C.; Gong, X.; Lee, K.; Heeger, A. J. Thermally stable, efficient polymer solar cells with nanoscale control of the interpenetrating network morphology. *Adv. Funct. Mater.* **2005**, *15*, 1617–1622.
6 Kim, J. Y.; Lee, K.; Coates, N. E.; Moses, D.; Nguyen, T.-Q.; Dante, M.; Heeger, A. J. Efficient tandem polymer solar cells fabricated by all-solution processing. *Science* **2007**, *317*, 222–225.
7 Peet, J.; Kim, J. Y.; Coates, N. E.; Ma, W. L.; Moses, D.; Heeger, A. J.; Bazan, G. C. Efficiency enhancement in low-bandgap polymer solar cells by processing with alkane dithiols. *Nat. Mater.* **2007**, *6*, 497–500.
8 Liang, Y.; Wu, Y.; Feng, D.; Tsai, S.-T.; Son, H.-J.; Li, G.; Yu, L. Development of new semiconducting polymers for high performance solar cells. *J. Am. Chem. Soc.* **2009**, *131*, 56–57.
9 Yoo, S.; Domercq, B.; Kippelen, B. Efficient thin-film organic solar cells based on pentacene/C_{60} heterojunctions. *Appl. Phys. Lett.* **2004**, *85*, 5427–5429.
10 Mayer, A. C.; Lloyd, M. T.; Herman, D. J.; Kasen, T. G.; Malliaras, G. G. Postfabrication annealing of pentacene-based photovoltaic cells. *Appl. Phys. Lett.* **2004**, *85*, 6272–6274.
11 Pandey, A. K.; Nunzi, J.-M. Efficient flexible and thermally stable pentacene/C_{60} small molecule based organic solar cells. *Appl. Phys. Lett.* **2006**, *89*, 213506.
12 Tang, C. W. Two-layer organic photovoltaic cell. *Appl. Phys. Lett.* **1986**, *48*, 183–185.
13 Halls, J. J. M.; Walsh, C. A.; Greenham, N. C.; Marseglia, E. A.; Friend, R. H.; Moratti, S. C.; Holmes, A. B. Efficient photodiodes from interpenetrating polymer networks. *Nature* **1995**, *376*, 498–500.
14 Yoo, S.; Potscavage, W. J., Jr.; Domercq, B.; Han, S.-H.; Li, T.-D.; Jones, S. C.; Szoszkiewicz, R.; Levi, D.; Riedo, E.; Marder, S. R.; Kippelen, B. Analysis of improved photovoltaic properties of pentacene/C_{60} organic solar cells: Effects of exciton blocking layer thickness and thermal annealing. *Solid-State Electron.* **2007**, *51*, 1367–1375.
15 Pettersson, L. A. A.; Roman, L. S.; Inganäs, O. Modeling photocurrent action spectra of photovoltaic devices based on organic thin films. *J. Appl. Phys.* **1999**, *86*, 487–496.
16 Peumans, P.; Yakimov, A.; Forrest, S. R. Small molecular weight organic thin-film photodetectors and solar cells. *J. Appl. Phys.* **2003**, *93*, 3693–3723.
17 Ramsdale, C. M.; Barker, J. A.; Arias, A. C.; MacKenzie, J. D.; Friend, R. H.; Greenham, N. C. The origin of the open-circuit voltage in polyfluorene-based photovoltaic devices. *J. Appl. Phys.* **2002**, *92*, 4266–4270.
18 Kietzke, T.; Egbe, D. A. M.; Hörhold, H.-H.; Neher, D. Comparative study of M3EH-PPV-based bilayer photovoltaic devices. *Macromolecules* **2006**, *39*, 4018–4022.
19 Rand, B. P.; Burk, D. P.; Forrest, S. R. Offset energies at organic semiconductor heterojunctions and their influence on the open-circuit voltage of thin-film solar cells. *Phys. Rev. B* **2007**, *75*, 115327.
20 Brumbach, M.; Placencia, D.; Armstrong, N. R. Titanyl phthalocyanine/C_{60} heterojunctions: Band-edge offsets and photovoltaic device performance. *J. Phys. Chem. C* **2008**, *112*, 3142–3151.
21 Brabec, C. J.; Cravino, A.; Meissner, D.; Sariciftci, N. S.; Fromherz, T.; Rispens, M. T.; Sanchez, L.; Hummelen, J. C. Origin of the open circuit voltage of plastic solar cells. *Adv. Funct. Mater.* **2001**, *11*, 374–380.
22 Gadisa, A.; Svensson, M.; Andersson, M. R.; Inganäs, O. Correlation between oxidation potential and open-circuit voltage of composite solar cells based on blends of polythiophenes/fullerene derivative. *Appl. Phys. Lett.* **2004**, *84*, 1609–1611.

23 Deng, X.; Zheng, L.; Yang, C.; Li, Y.; Yu, G.; Cao, Y. Polymer photovoltaic devices fabricated with blend MEHPPV and organic small molecules. *J. Phys. Chem. B* **2004**, *108*, 3451–3456.

24 Scharber, M. C.; Mühlbacher, D.; Koppe, M.; Denk, P.; Waldauf, C.; Heeger, A. J.; Brabec, C. J. Design rules for donors in bulk-heterojunction solar cells - towards 10% energy-conversion efficiency. *Adv. Mater.* **2006**, *18*, 789–794.

25 Kooistra, F. B.; Knol, J.; Kastenberg, F.; Popescu, L. M.; Verhees, W. J. H.; Kroon, J. M.; Hummelen, J. C. Increasing the open circuit voltage of bulk-heterojunction solar cells by raising the LUMO level of the acceptor. *Org. Lett.* **2007**, *9*, 551–554.

26 Yoo, S.; Domercq, B.; Kippelen, B. Intensity-dependent equivalent circuit parameters of organic solar cells based on pentacene and C_{60}. *J. Appl. Phys.* **2005**, *97*, 103706.

27 Xue, J.; Uchida, S.; Rand, B. P.; Forrest, S. R. 4.2% efficient organic photovoltaic cells with low series resistances. *Appl. Phys. Lett.* **2004**, *84*, 3013–3015.

28 Sharma, A.; Haldi, A.; Hotchkiss, P. J.; Marder, S. R.; Kippelen, B. Effect of phosphonic acid surface modifiers on the work function of indium tin oxide and on the charge injection barrier into organic single-layer diodes. *J. Appl. Phys.* **2009**, *105*, 074511.

29 Sharma, A.; Hotchkiss, P. J.; Marder, S. R.; Kippelen, B. Tailoring the work function of indium tin oxide electrodes in electrophosphorescent organic light-emitting diodes. *J. Appl. Phys.* **2009**, *105*, 084507.

30 Sharma, A.; Haldi, A.; Potscavage, W. J., Jr.; Hotchkiss, P. J.; Marder, S. R.; Kippelen, B. Effects of surface modification of indium tin oxide electrodes on the performance of molecular multilayer organic photovoltaic devices. *J. Mater. Chem.* **2009**, 5298–5302.

31 Pandey, A. K.; Shaw, P. E.; Samuel, I. D. W.; Nunzi, J.-M. Effect of metal cathode reflectance on the exciton-dissociation efficiency in heterojunction organic solar cells. *Appl. Phys. Lett.* **2009**, *94*, 103303.

32 Kao, P.-C.; Chu, S.-Y.; Liu, S.-J.; You, Z.-X.; Chuang, C.-A. Improved performance of organic light-emitting diodes using a metal-phthalocyanine hole-injection layer. *J. Electrochem. Soc.* **2006**, *153*, H122–H126.

33 Tanaka, H.; Yasuda, T.; Fujita, K.; Tsutsui, T. High efficiency polarization-sensitive organic photovoltaic devices. *Appl. Phys. Lett.* **2006**, *88*, 253506.

34 Hill, I. G.; Hwang, J.; Kahn, A.; Huang, C.; McDermott, J. E.; Schwartz, J. Energy level alignment between 9-phosphonoanthracene self-assembled monolayers and pentacene. *Appl. Phys. Lett.* **2007**, *90*, 012109.

35 Potscavage, W. J., Jr.; Yoo, S.; Kippelen, B. Origin of the open-circuit voltage in multilayer heterojunction organic solar cells. *Appl. Phys. Lett.* **2008**, *93*, 193308.

36 Drori, T.; Sheng, C.-X.; Ndobe, A.; Singh, S.; Holt, J.; Vardeny, Z. V. Below-gap excitation of π-conjugated polymer-fullerene blends: Implications for bulk organic heterojunction solar cells. *Phys. Rev. Lett.* **2008**, *101*, 037401.

37 Molodtsova, O. V.; Knupfer, M. Electronic properties of the organic semiconductor interfaces CuPc/C_{60} and C_{60}/CuPc. *J. Appl. Phys.* **2006**, *99*, 053704.

38 Tang, J. X.; Zhou, Y. C.; Liu, Z. T.; Lee, C. S.; Lee, S. T. Interfacial electronic structures in an organic double-heterostructure photovoltaic cell. *Appl. Phys. Lett.* **2008**, *93*, 043512.

39 Brédas, J.-L.; Beljonne, D.; Coropceanu, V.; Cornil, J. Charge-transfer and energy-transfer processes in π-conjugated oligomers and polymers: A molecular picture. *Chem. Rev.* **2004**, *104*, 4971–5003.